Energy & Environmental Science

Accepted Manuscript

This article can be cited before page numbers have been issued, to do this please use: S. Ye, F. Luo, Q. Zhang, P. Zhang, T. Xu, D. He, L. Guo, Y. Zhang, C. He, X. Ouyang, Q. Wang, M. Gu, J. Liu and X. Sun, *Energy Environ. Sci.*, 2019, DOI: 10.1039/C8EE02888E.

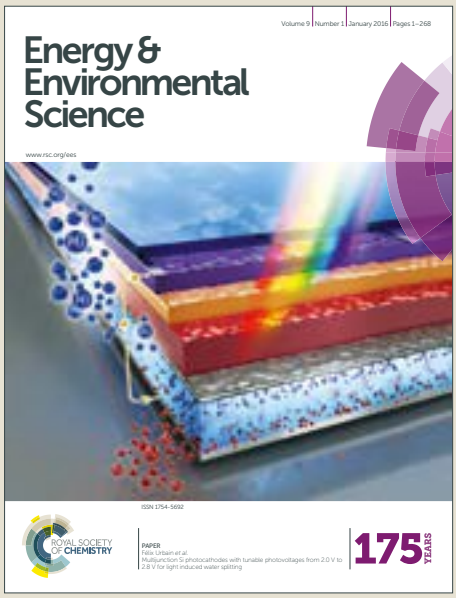

ROYAL SOCIETY OF CHEMISTRY

rsc.li/ees

View Article Online
DOI: 10.1039/C8EE02888E

Journal Name

ARTICLE

Highly stable single Pt atomic sites anchored on aniline-stacked graphene for the hydrogen evolution reaction

Received 00th January 20xx,
Accepted 00th January 20xx

DOI: 10.1039/x0xx00000x

www.rsc.org/

Shenghua Ye,‡[a] Feiyan Luo,‡[a] Qianling Zhang, ‡[a] Pingyu Zhang,[a] Tingting Xu,[a] Dongsheng He,[c] Licheng Guo,[a] Yu Zhang,[a] Chuanxin He,[a] Xiaoping Ouyang,[d] Qi Wang,[c] Meng Gu,*[c] Jianhong Liu*[a] and Xueliang Sun*[b]

Developing efficient and cost-effective electrocatalysts for hydrogen evolution reaction (HER) is highly desired for hydrogen economy. In this study, we developed a facile microwave reduction method to synthesize single Pt atoms anchored on aniline-stacked graphene (Pt SASs/AG) with outstanding HER performances. The Pt SASs/AG presents excellent HER activity with η = 12 mV at 10 mA cm^{-2} and mass current density of 22400 Ag$^{-1}_{Pt}$ at η =50 mV, which is 46 times higher than that of commercial 20 wt% Pt/C. Moreover, the Pt SASs/AG catalyst is highly active and more stable than Pt/C. X-ray absorption fine spectroscopy (XAFS) and density functional theory (DFT) calculations elucidated that atomically isolated Pt coordinating with nitrogen of aniline optimized the electronic structure of Pt and hydrogen adsorption energy, eventually promoted HER activity. This study opens up a new avenue for the development of single Pt atomic electrocatalyst with high activity and stability.

Broader context: Exploring low-cost and efficient electrocatalysts for hydrogen evolution reaction (HER) from water splitting is important for developing hydrogen production which is a renewable and clean fuel thus has great potential in solving the energy crisis. Precious metal Pt is still the most active candidate with negligible overpotential for HER at present, but high-cost and limited reserve of Pt hinders the commercialization of Pt-based catalysts, bringing an urgent goal of lowing Pt loading without sacrifice of HER catalytic activity. Single atomic catalysts (SACs) featured with isolated catalytic sites provide an alternative way for solving the above conflicts. However, harsh preparation conditions (calcination or H_2 reduction) and excess precursors usually result in agglomeration of single atomic sites, stability of SACs is a great challenge. Herein, we for the first time present a mild and facile strategy involves aniline anchoring and microwave reduction to exclusively disperse Pt atomic sites on graphene. Importantly, we demonstrate that d-electron structure of Pt atoms can be modified by aniline molecules, which is crucial for improvement of HER activities. This study opens up a new avenue of developing SACs and brings new understanding about catalytic performances of SACs.

Introduction

Hydrogen is one of the promising candidates for green energy applications owing to its high energy density, low-pollution and greenhouse gas-free emission.[1-3] Along with the popularization of electric energy, large-scale water splitting to generate high-purity hydrogen has attracted considerable attentions and many electrocatalysts for the hydrogen evolution reaction (HER) have been developed in recent years.[4]

Although Pt-based catalysts are the most active catalysts for HER,[5-6] the global reserves and high cost of Pt hinder their large-scale application.[7-9] In recent years, numerous catalysts made of non-noble transition metals were explored for HER, such as transition metal phosphides,[10-12] sulfides,[13-16] nitrides,[17] selenides,[18-20] and carbrides[21] due to their improved HER performance. Unfortunately, these transition metal catalysts usually have higher overpotential and lower catalytic performances than Pt-based catalysts, which makes Pt still irreplaceable at present. It is important to find a method for drastically reducing Pt loading and improving catalytic activity in the meantime.

Recently, single-atom catalysts have attracted considerable attention because of their excellent catalytic performances.[22-23] Zhang et al. for the first time demonstrated that single Pt atoms dopants in FeO_x were well suited for CO oxidation and nitroarene hydrogenation.[24] Then other kinds of single-atoms dispersed on g-C_3N_4,[25] ZnO,[26] Al_2O_3,[27] MoS_2,[28] CeO_2,[29] MoC,[30] and carbon substrates derived from polymers or metal-organic framework (MOF) [31-38] were developed for potential electrocatalysts. However, the preparation of single-atom catalysts requires harsh condition and precise precursor concentration. Calcination or H_2 reduction

[a] College of Chemistry and Environmental Engineering, Shenzhen University, Shenzhen, 518060, P. R. China
[b] Department of Mechanical and Materials Engineering, University of Western Ontario, London, Ontario N6A 5B9, Canada
[c] Materials Characterization and Preparation Center, South University of Science and Technology of China, Shenzhen, 518055, P. R. China
[d] School of Materials Science and Engineering, Xiangtan University, Xiangtan, 411105, P. R. China

‡These authors have contributed equally.

Electronic Supplementary Information (ESI) available: [details of anysupplementary information available should be included here]. See DOI: 10.1039/x0xx00000x

and excess precursors usually result in single atomic sites forming clusters even nanoparticles during the preparation.

In this study, single Pt atomic sites anchored on aniline-stacked graphene (denoted as Pt SASs/AG) were synthesized via a mild and facile aniline anchoring and microwave reduction. The as-prepared catalyst with Pt loading of 0.44 wt% presents unexpectedly high catalytic activity with negligible onset potential and delivers overpotential of 12 mV at 10 mA cm^{-2} in 0.5 M H_2SO_4 solution. Moreover, it displays excellent stability and durability without any obvious current deterioration and structure change during long-term catalysis. X-ray absorption fine spectroscopy (XAFS) suggests that a Pt site coordinates with four aniline molecules, density functional calculation (DFT) suggests that the electronic structure of Pt is altered by aniline molecules, which makes single Pt atomic sites have appropriate hydrogen adsorption energy. Furthermore, the Pt SASs/AG greatly improves the utilization of catalytic sites, the excellent conductivity of graphene and hydrophilic catalyst interface also contribute to its excellent HER performances.

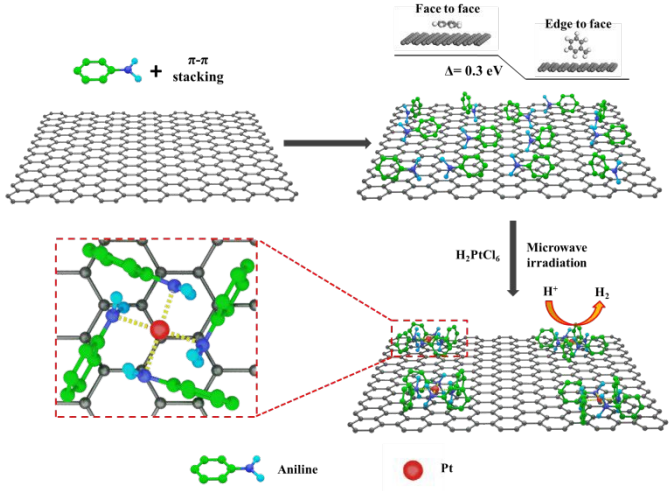

Fig. 1 Synthetic scheme of Pt SASs/AG.

Rusult and Discussion

The preparation of Pt SASs/AG is depicted in Fig. 1. Graphene was functionalized by the aniline molecules owing to the π–π interaction, which made the graphene be hydrophilic (the water-contact angle before and after aniline stacking is shown in Fig. S3, ESI†) and could be uniformly re-dispersed in the aqueous solution (Fig. S4, ESI †). Moreover, previous researches reveal that π-π interaction is strong thus preventing stacked molecules from detaching into solution during electrocatalysis.[39-40] In particular, aromatic π-π interactions have two configurations: face-to-face and edge-to-face, their absorption energies are investigated by density functional theory (DFT), the results indicate that aniline stacked on graphene by edge-to-face configuration has significant lower energy than that of face-to-face configuration (Fig. 1), therefore, edge-to-face configuration is thermodynamics preferred. Subsequently, the H_2PtCl_6 solution (1 mL, 0.0193 mol L^{-1}) was added to the above solution with stirring for 2 h. During this process, pH of the solution is 2.26, which is much lower than pK_a (4.62) of conjugate acid of aniline (The pK_b of aninile is 9.38), thus partial $-NH_2$ of aninilie was protonated to form $-NH_3^+$, graphene was positively charged and $PtCl_6^{2-}$ ions were anchored on AG by electrostatic force to keep the charge balance. Eventually, the anchored $PtCl_6^{2-}$ ions were reduced to single Pt atomic sites by microwave irradiation.

The TEM images of Pt SASs/AG (Fig. 2a) demonstrate that the wrinkled structure of graphene is well maintained in Pt SASs/AG. Elemental mapping of N and Pt confirms that the aniline and Pt are uniformly dispersed throughout the graphene in Pt SASs/AG (Fig. 2b). No nanoparticles even clusters are seen on the surface of Pt SASs/AG (Fig. 2c, d). Aberration-corrected high-angle annular dark-field scanning transmission electron microscopy (AC HAADF-STEM) was used to characterize the dispersion of Pt in Pt SASs/AG. As illustrated in Fig. 2e and f, single Pt atomic sites (bright dots in Fig. 2e, f) were anchored on the graphene without visible agglomeration, suggesting that atomically isolated Pt sites were obtained. The percentage of Pt measured by inductively coupled plasma-mass spectroscopy (ICP-MS) is 0.44 wt% for Pt SASs/AG.

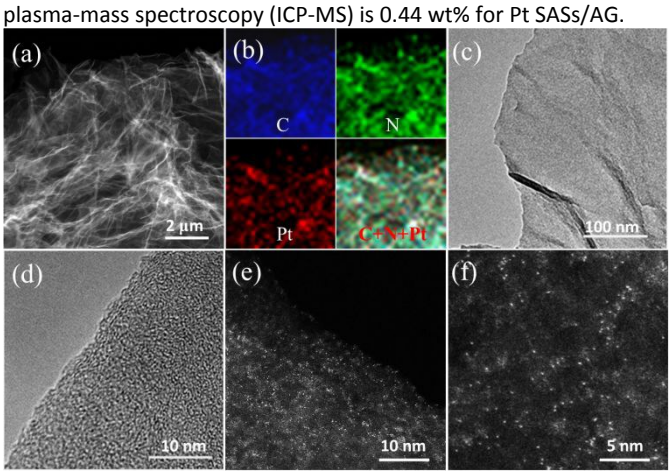

Fig. 2 (a) Low magnified dark field TEM image and corresponding (b) elemental mapping of C, N and Pt of Pt SASs/AG; (c) high magnified bright field TEM image and (d) HR-TEM image of Pt SASs/AG; (e-f) AC HAADF-STEM images of Pt SASs/AG.

X-ray diffraction pattern of Pt SASs/AG (Fig. S6, ESI†) suggests that crystalline Pt is absent. Only C, N and O are observed in the X-ray photoelectron spectroscopy (XPS) of AG (Fig. S7, ESI†). The C 1s spectrum suggests the presence of sp^2 hybridized carbon atoms, pointing to the planar graphene with low defect concentration. The O 1s peak at ~532 eV is ascribed to the adsorbed H_2O.[41-42] The trace amounts of N are originated from $-NH_2$ of stacked aniline. Similar results, except trace amounts of Pt, are found in Pt SASs/AG (Fig. S8, ESI †). The content of N is also calculated to be 2.75 at%. Furthermore, the Pt 4f spectrum of Pt SASs/AG in Fig. 3a suggests that the binding energy of Pt (71.55 eV) is close to Pt^0 at 71.11 eV with a slightly positive shift but far lower than that of Pt before microwave irradiation at 72.8 eV (Fig. S9e ESI †), suggesting that H_2PtCl_6 has been reduced and the strong interaction between Pt and aniline forms $Pt^{\delta+}$. X-ray near-edge absorption spectra (XANES) for Pt L_3-edge of Pt SASs/AG, Pt/C, and Pt foil are depicted in Fig 3b. It has been reported that the white line (WL) is directly related to the unoccupied density of states of the Pt 5d orbits.[43-44] The intensive WL of Pt SASs/AG suggests the increased vacancies of d-orbitals of Pt and agrees with the XPS results. Extended X-ray absorption fine-structure spectroscopy (EXAFS) of Pt SASs/AG, Pt/C, and Pt foil spectra are illustrated in Fig. S10 ESI†. The Pt SASs/AG

has different oscillations from Pt/C, suggesting different mode in coordination. The corresponding k^3-weight Fourier transforms (FTs) of the EXAFS spectra are depicted in Fig. 3c. Pt SASs/AG has only one peak corresponding to the Pt–N first coordination shell and no Pt–Pt coordination peak is detected. Combined with the AC HAADF-STEM results, it can be confidently concluded that the atomically isolated Pt sites are dispersed on graphene. The obtained coordination number of Pt–N is about 4 (Table S1, supporting information), the fitting curve is exhibited in Fig. 3d, suggesting that atomically isolated Pt is coordinated by four aniline molecules to form Pt–N configuration, as illustrated in inset graph of Fig. 3d.

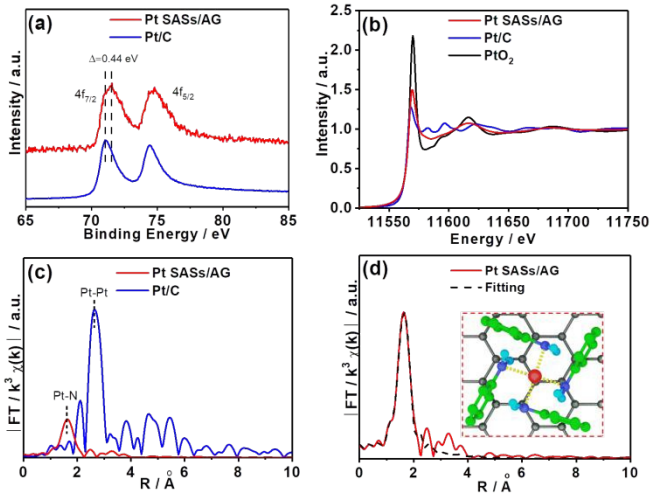

Fig. 3 (a) Pt 4f spectra of Pt SAS/AG and Pt/C; (b) XANES and (c) FT-EXAFS of the Pt L_3-edge of Pt SASs/AG and Pt/C (without phase correction); (d) Corresponding EXAFS fitting curve of Pt SASs/AG R-space, the inset of graph is the model of Pt SASs/AG.

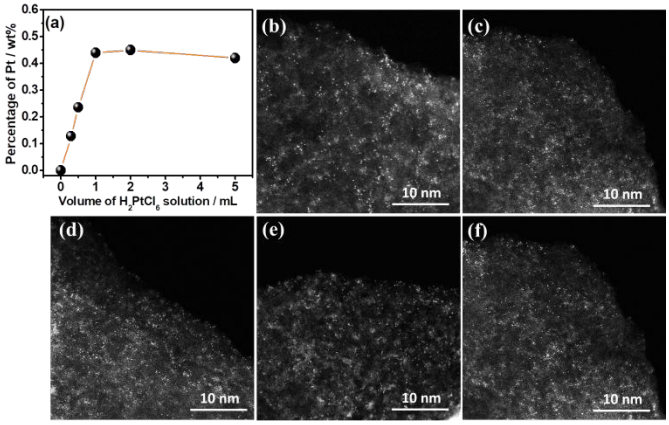

Fig. 4 (a) Mass percentages of Pt in Pt SASs/AG prepared by H_2PtCl_6 solution (0.3 mL, 0.5 mL, 1 mL, 2 mL, and 5mL)， AC-HAADF-STEM images of prepared by (b) 0.3 mL, (c) 0.5 mL, (d) 1 mL, (f) 2 mL, and (f) 5mL H_2PtCl_6 solution respectively.

Moreover, a series of Pt SASs/AG prepared by different volumes (0–5 mL) of H_2PtCl_6 solution were also synthesized and the loading amounts of Pt measured by ICP-MS are depicted in Fig. 4a. The percentage of Pt increased in the range between 0 and 0.44 wt% and then remained constant even over 1 mL H_2PtCl_6 solution. AC-HAADF-STEM images (Fig. 4b-f) also suggest that Pt in all above samples is presented in single atomic sites without visible agglomeration, indicating that the aniline anchoring can exclusively form single atomic sites even if excessed metallic precursor are used, unlike previous reports that clusters are easy to form and the precise precursor are needed, this advantage benefits by two aspects: Firstly, maximum protonation of aniline results in the maximum loading of $PtCl_6^{2-}$, thus the excess Pt cannot be anchored, which guarantees Pt clusters or nanoparticles cannot be formed, and 0.44 wt% is the saturate point of Pt SASs; Secondly, microwave reduction is a mild synthesis method without extreme condition such as high temperature, which protects Pt SASs from sintering.

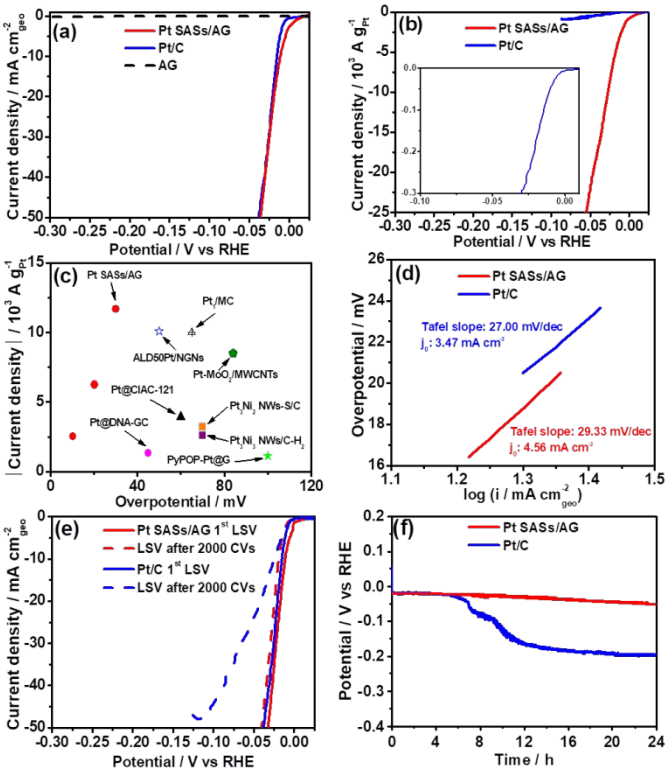

Fig. 5 LSV curves of Pt SASs/AG and Pt/C with current density normalized to the (a) geometry area and (b) mass of Pt in 0.5 M H_2SO_4 at 2 mV s^{-1} (Inset graph is enlarged curves of Pt/C), respectively; (c) mass activities of Pt SASs/AG, Pt/C, and other state-of-the-art Pt-based catalysts in 0.5 M H_2SO_4; (d) Tafel plots of Pt SASs/AG and Pt/C; (e) LSV curves of Pt SASs/AG before and after 2000 cycles; (f) chronopotentiometric curves of Pt SASs/AG and Pt/C at 10 mA cm^{-2} in 0.5 M H_2SO_4 solution.

The electrocatalytic activity of Pt SASs/AG for HER in 0.5 M H_2SO_4 solution was evaluated by linear sweep voltammetry (LSV) at a scan rate of 2 mV s^{-1} with iR correction. The HER activity of Pt SASs/AG samples, prepared at different concentrations of H_2PtCl_6 solution, is depicted in Fig. S11 ESI†. The results show that the tendency are the same as Fig. 4a and the amount of Pt loading as low as 0.44 wt% (1 mL H_2PtCl_6 solution) has the highest HER activity, thus the Pt SASs/AG with 0.44 wt% of Pt is selected as a representative to further study its catalytic performances.

LSV curves of Pt SASs/AG, AG and commercial 20%wt Pt/C with iR correction are depictied in Fig. 5a (LSV curves without iR correction are shown in Fig. S12, ESI†), the Pt SASs/AG has negligible onset potential. At the current density of 10 mA cm^{-2}, the Pt SASs/AG displays overpotential of 12 mV, which is better than 15 mV of 20 wt% Pt/C. To further compare the electrocatalytic

activities of Pt SASs/AG and 20 wt% Pt/C, the current densities are normalized to the mass of Pt as depicted in Fig. 5b. The mass current density of Pt SASs/AG reaches 22400 A g^{-1}_{Pt} at η = 50 mV, which is 46 times higher than that of 20 wt% Pt/C. Fig. 5c illustrates the mass activities of different Pt-based HER catalysts. Pt SASs/AG has superior mass activity comparing to the other state-of-the-art Pt-based catalysts[45-50] and current single Pt atomic catalysts,[51-53] indicating that the excellent catalytic activity with low consumption of precious Pt is due to the unique single atomic structure.

Tafel slopes are calculated to identify the HER mechanism on the electrocatalysts (Fig. 5d). The Tafel slope of Pt SASs/AG is 29.33 mV dec^{-1}, very close to 27.00 mV dec^{-1} of Pt/C, suggesting a typical Tafel mechanism for HER.[54] By extrapolating the Tafel plots for η at 0 V, the exchange current density (j_0) of Pt SASs/AG is calculated to be 4.56 mA cm^{-2}, which is slightly higher than that of Pt/C (3.47 mA cm^{-2}), suggesting the high activity of Pt SASs/AG.

Stability is an important issue in the development of single atomic electrocatalysts. The cyclic stability of Pt SASs/AG and Pt/C were evaluated by comparing the LSV curves before and after 2000 cycles (from +0.05 to -0.25 vs RHE with 50 mV s^{-1}) in 0.5 M H_2SO_4 solution, as shown in Fig. 5e. The Pt SASs/AG presents negligible catalytic activity decay, while the 20 wt% commercial Pt/C deteriorates seriously after 2000 cyclic voltammetry sweeps. To further assess the long-term durability of Pt SASs/AG and Pt/C, chronopotentiometric measurement at current density of 10 mA cm-2 was performed. The chronopotentiometric curves (Fig. 5f) of Pt SASs/AG and Pt/C suggest that Pt SASs/AG maintains its high catalytic activity and stability during long-term electrolysis, whereas Pt/C appears obvious attenuation. After durability testing, it can be obviously seen that serious agglomeration occurs in Pt/C (Fig. S13, ESI †), thus the decreased activity of Pt/C can be attributed to the irreversible agglomeration of Pt nanoparticles driven by Ostwald ripening. By contrast, TEM image of Pt SASs/AG after durability test (Fig. S14a, ESI †) shows that no cluster or nanoparticle can be observed on graphene, but N and Pt are still dispersed uniformly on graphene (Fig. S14b-f, ESI †), the AC HAADF-STEM image shown in Fig. S14g ESI † suggests that atomically dispersed Pt can be clearly observed in most areas of the sample even after long-term durability testing. Moreover, the electronic and coordinative structures of Pt SASs/AG still remain unchanged, as depicted in Fig. S15 ESI † and Table S2 ESI †. The above sharp contrasts indicate that Pt SASs/AG has outstanding stability, which is ascribed to the strong interaction between Pt and aniline and the strong π–π interaction from graphene.

The origination of excellent HER activity of Pt SASs/AG was further investigated.

Visually, atomically dispersed Pt sites maximize their utilization thus greatly decrease the precious metal loading and increase the mass activity significantly, and the aniline anchoring prevents Pt sites from aggregating during catalytic process, thus improves the stability.

To provide a theoretical understanding of the effect of aniline, the DFT calculation was carried out to study the structure-property correlation between Pt coordination and electrocatalytic activity. Fig. 6a-c show three typical structures (top view) of Pt (111), single Pt atom absorbed on graphene (Pt_{ab}/G), Pt SASs/AG, and their partial density of states (PDOS) of 5d orbits are shown in Fig. 6d-f respectively (The total DOS are shown in Fig. S18 ESI †). Clearly, Pt_{ab}/G and Pt SASs/AG largely retain the isolated atomic orbital characteristics comparing to the Pt (111), and the PDOS of Pt SASs/AG is greatly different from that of Pt_{ab}/G, indicating that the

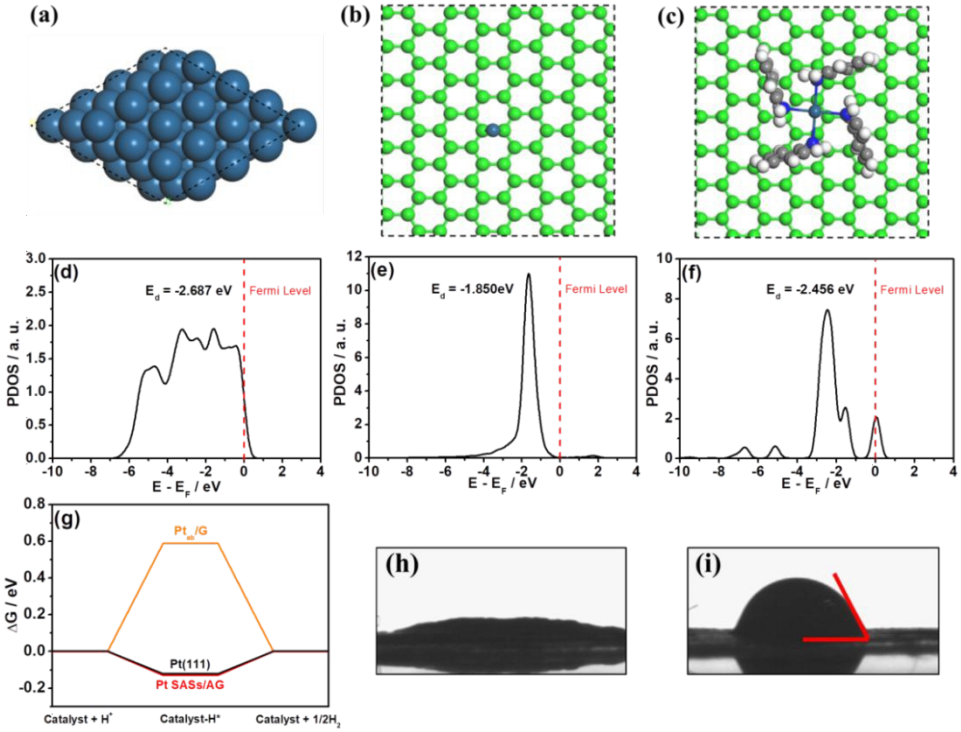

Fig. 6 DFT calculation models (top views) of (a) Pt (111), (b) Pt_{ab}/G and (c) Pt SASs/AG; PDOS of 5d orbits of Pt in (d) Pt (111), (e) Pt_{ab}/G and (f) Pt SASs/AG; (g) Calculated free energy diagram of HER for Pt (111), Pt_{ab}/G and Pt SASs/AG; Water-contact angle of (h) Pt SASs/AG and (i) Pt/C.

View Article Online
DOI: 10.1039/C8EE02888E

Journal Name

ARTICLE

electronic structure of Pt can be significantly affected by the adjoining aniline molecules. The d-band center model is a good descriptor of the adsorbate-metal interaction, the downshift of the d-band center decreases the adsorption energy of H and meanwhile facilitates the desorption of H from the catalyst surface for HER catalysis.[55] As a result, the d-band center of Pt in Pt_{ab}/G is calculated to be -1.805 eV, which is higher than -2.687 eV of Pt in Pt (111) (Fig. 6 d-e), implying that the single Pt atom adsorbed on graphene is inactive for HER. However, when the single Pt atom is anchored by aniline molecules, its d-band center downshifts to -2.465 eV, which is very close to that of Pt (111) (Fig. 6f), indicating that the synergetic effect of aniline and Pt is crucial for HER activity.

On the other hand, DOS near Fermi level is also crucial for the adsorbates (e.g. H^+ for HER) to interact with the catalytic sites, the higher electron densities near the Fermi level can facilitate H^+ absorption.[56-57] As a result, the DOS near Fermi level of Pt in Pt_{ab}/G is absent, suggesting that Pt_{ab}/G is inactive for HER once again. Nevertheless, the DOS near Fermi level of Pt in Pt SASs/AG is as large as that of Pt in Pt (111), indicating that the special coordination environment can effectively improve the d-electrons of Pt domination near the Fermi level and optimize the catalytic activity.

Furthermore, the hydrogen adsorption free energy (ΔG_H*) is also a key descriptor for HER activity. HER can be summarized in a three-state diagram consisting of initial H^+, intermediate H atoms, and final H_2 as the product. The optimal ΔG_H* of the catalyst-H* is close to 0 eV because negative ΔG_H* or positive ΔG_H* on the catalyst will result in poor HER activity owing to the difficulties in intermediate H atoms desorption and generation, respectively.[58-59] The simplified DFT models of Pt SASs/AG, Pt, and aniline are depicted in Fig. S19 ESI†. The ΔG_H* diagrams of Pt SASs/AG, Pt_{ab}/G, and Pt (111) are shown in Fig. 6g. Obviously, the calculated ΔG_H* of Pt_{ab}/G is 0.587 eV, suggesting that single Pt atom alone on graphene is HER inactive. But the ΔG_H* of Pt SASs/AG is calculated to be -0.127 eV, which is almost the same as -0.121 eV of Pt (111), confirming that aniline coordinating endows the single Pt atomic site with HER active, it is well coincide with the PDOS results.

Moreover, the electrical conductivities of Pt SASs/AG and Pt/C were determined by the four-probe method. The Pt SASs/AG resistivity is 1.22×10^{-2} Ω cm, which is remarkably lower than that of 20 wt% Pt/C (1.23 Ω cm) owing to the higher conductivity of graphene than amorphous carbon which favouring electron transport and reducing the overpotential. In addition, the water-contact angles of Pt SASs/AG and 20 wt% Pt/C shown in Fig. 6h–i suggest that the interface of Pt SASs/AG is more hydrophilic than 20 wt% Pt/C owing to the stacking of aniline molecules on graphene. The hydrophilic interface ensures that the catalyst can be wetted and penetrated by the electrolyte adequately, which facilitates the diffusion and transport of active species.

Conclusions

In summary, we developed a facile aniline anchoring and microwave reduction method to synthesize single Pt atomic sites anchoring on aniline-stacked on graphene (Pt SASs/AG) for hydrogen evolution reaction (HER). Pt SASs/AG presents outstanding HER catalytic performances with higher specific current density and mass current density at lower overpotential and superior stability than 20 wt% Pt/C. The excellent HER activity of Pt SASs/AG is attributed to (1) the atomically dispersed Pt sites that maximized the utilization of catalytic sites; (2) the d-band center and density of state near Fermi level of Pt atoms were modulated by anilines, thus the Gibbs free energy of absorbed H was optimized; (3) the excellent electrical conductivity of the graphene; (4) the improved hydrophilicity of catalyst interface owing to the aniline stacking on graphene by π–π interaction. This study develops a new opportunity for the preparation and application of high-efficiency and stable single Pt atomic sites for HER catalysts.

Experimental Methods

Materials

The chemical reagents were all analytical grade and were directly utilized without any purification. Chloroplatinic acid hexahydrate (H_2PtCl_6) and aniline were purchased from Aladdin. Ethylene glycol and ethanol anhydrous were purchased from Macklin. Single-layer graphene was produced by the Shenzhen Eigan-equation Graphene Technology Co. Ltd (Shenzhen, China) via liquid sintering of the liquid acrylonitrile homopolymer precursor.

Catalyst preparation

For the preparation of Pt SASs/AG, 10 mg graphene was mixed with 1 mL aniline and was shook to form a black paste. Subsequently, 50 mL of deionized water was used to uniformly disperse the paste. Then, the dispersion was filtered to obtain a black paste, re-dispersed in the deionized water, and filtered several times to remove the unstacked aniline, the aniline-stacked graphene was obtained. Aniline-stacked graphene was re-dispersed in 50 mL deionized water to form an uniform dispersion, variable volumes of 0.0193 mol L^{-1} H_2PtCl_6 was added into the dispersion and vigorously stirred for 2h. Then, the dispersion was filtered and redispersed in deionized water. This step was repeated more than ten times to thoroughly remove the unanchored $PtCl_6^{2-}$ ions. The final product was dried in a vacuum oven at 60 ℃ overnight. The above product of the previous steps was re-dispersed in 10 mL of ethylene glycol and subjected to 800 W microwave irradiation for 2 min. After being cooled to room temperature, the sample was washed with deionized water and dried in vacuum oven at 60 ℃

overnight to obtain the Pt SASs/AG. For the preparation of AG, the same scheme as for Pt SASs/AG was followed except the addition of H_2PtCl_6 and the microwave irradiation.

Catalyst characterization

The morphologies of the samples were characterized by transmission electron microscopy (TEM) (JEM-2010HR and Tecnai F30 S-TWIN). Chemical-state analysis of samples was determined by X-Ray photoelectron spectroscopy (XPS) using an ESCAKAB 250 X-Ray photoelectron spectrometer. All the peaks were corrected by the C 1s line at 284.4 eV as standard, followed by curve fitting and background subtraction. Chemical composition was determined by inductively coupled plasma-atomic emission spectrometry (ICP-AES) with a TJA IRIS (HR) spectrometer. The catalysts were also characterized by Raman spectroscopy (Renishaw). XANES measurements of the Pt L-edge were conducted on the 06ID superconducting wiggler-sourced hard X-ray microanalysis beamline at the 1W1B station of Beijing Synchrotron Radiation Facility (BSRF). Spectra for each sample were collected in transmission mode for comparison and monochromatic energy calibration. The single Pt atoms were measured by aberration-corrected high-angle annular dark-field scanning transmission electron microscopy (AC HAADF-STEM) (Titan Cubed Themis G20).

Electrochemical measurement

Electrochemical measurements were performed with a CHI 660E electrochemical analyzer (CH Instruments, Inc., Shanghai) in a standard three-electrode system, using sample-coated glass carbon electrodes as the working electrode, a graphite rod as the counter electrode, and a saturated calomel electrode (SCE) as the reference electrode. The loading of catalysts is 7.07 mg cm^{-2}. In all measurements, the SCE reference electrode was calibrated with respect to the reversible hydrogen electrode (RHE). In H_2 saturated 0.5M H_2SO_4, E (RHE) = E (SCE) + 0.242 V. LSV measurements were conducted in electrolyte at scan rate of 2 mV s^{-1}. Cyclic voltammetry was run at a scan rate of 50 mV s^{-1}.

Computational method

The first principles calculations in the framework of density functional theory including structural and electronic performances were carried out based on the Cambridge Sequential Total Energy Package known as CASTEP.[60] The exchange – correlation functional under the generalized gradient approximation (GGA)[61] with norm-conserving pseudopotentials and Perdew–Burke–Ernzerhof functional was adopted to describe the electron–electron interaction.[62] An energy cutoff of 750 eV was used and a k-point sampling set of 5 x 5 x 1 was tested to be converged. A force tolerance of 0.01 eV $Å^{-1}$, energy tolerance of $5.0x10^{-7}$ eV per atom and maximum displacement of $5.0x10^{-4}$ Å were considered. Each atom in the storage models is allowed to relax to the minimum in the enthalpy without any constraints. The vacuum space along the z direction is set to be 15 Å, which is enough to avoid interaction between the two neighboring images. The Grimme method for DFT-D2 correction is considered for all calculations.[63] The Pt on graphite with and without modified by C6 have been built, then the H atom has been absorbed on the top of Pt atom, and all atoms of systems are relaxed. The Pt (111) surface has been also built with the three bottom atomic layers are fixed and top three atomic layers are relaxed.

View Article Online
DOI: 10.1039/C8EE02888E

Adsorption energy ΔE of H atom on the surface of substrates was defined as:

$$\Delta E = E^*_H - (E^* + E_H)$$

where *H and * denote the adsorption of H atom on substrates and the bare substrates, EH denotes the half of energy of H_2.

Free energy change ΔG of the reaction was calculated as the difference between the free energies of the initial and final states as shown below:

$$\Delta G = \Delta E + \Delta ZPE - T\Delta S$$

where E is the calculated energy by DFT, ZPE is the zero point energy, S denotes the entropy, The value of (ΔZPE- TΔS) is 0.24 eV,[63] ΔG= ΔE + 0.24eV.

Conflicts of interest

There are no conflicts to declare.

Acknowledgements

We thank the NSFC (No. 21571131) and Key Project of Natural Science Foundation of Guangdong Province (No. 2014A030311028) for JL, Shenzhen Basic Research Layout Project (No. 20170447) and Major Programs for Science and Technology Development of Shenzhen (No. XCL201110060) for QZ. Thanks Dr D.-S He for assistance with AC HAADF-STEM measurement.

References

1 J. Yang, F. Zhang, X. Wang, D. He, G. Wu, Q. Yang, X. Hong, Y. Wu and Y. Li, *Angew. Chem. Int. Ed.* 2016, **55**, 12854–12858.
2 B. W. Hao, Y. X. Bao, Y. Le, X. Y. Yu and X. W. Lou, *Nat. Commun.* 2015, **6**, 6512.
3 J. Staszakjirkovský, C. D. Malliakas, P. P. Lopes, N. Danilovic, S. S. Kota, K. C. Chang, B. Genorio, D. Strmcnik, V. R. Stamenkovic and M. G. Kanatzidis, *Nat. Mater.* 2015, **15**, 197.
4 P. Munnik, P. E. de Jongh and K. P.de Jong, *Chem. Rev.* 2015, **115**, 6687-6718.
5 J. K. Norskov and C. H.Christensen, *Science* 2006, **312**, 1322–1323.
6 L. Zhang, L. T. Roling, X. Wang, M. Vara, M. Chi, J. Liu, S. -I. Choi, J. Park, J. A. Herron, Z. Xie, M. Marvrikakis and Y. N. Xia, *Science* 2015, **349**, 412–416.
7 G. Li, X. Wang, J. Fu, J. Li, M. G. Park, Y. Zhang, G. Lui and Z. Chen, *Angew. Chem. Int. Ed. Engl.* 2016, **55**, 4977–4982.
8 E. J. Popczun, C. G. Read, C. W. Roske, N. S. Lewis and R. E. Schaak, *Angew. Chem. Int. Ed.* 2014, **126**, 5531–5534.
9 L. Liao, S. Wang, J. Xiao, X. Bian, Y. Zhang, M. D. Scanlon, X. Hu, Y. Tang, B. Liu and H. H. Girault, *Energy Environ. Sci.* 2013, **7**, 387–392.
10 E. J. Popczun, J. R. McKone, C. G. Read, A. J. Biacchi, A. M. Wiltrout, N. S. Lewis and R. E. Schaak, J. Am. Chem. Soc. 2013, **135**, 9267–9270.
11 Q. Liu, J. Tian, W. Cui, P. Jiang, N. Cheng, A. M. Asiri and X. Sun, *Angew. Chem. Int. Ed.* 2014, 126, 6710–6714.

DOI: 10.1039/C8EE02888E

12 M. Cabán-Acevedo, M. L. Stone, J. Schmidt, J. G. Thomas, Q. Ding, H. -C. Chang, M. -L. Tsai, J.-H. He and S. Jin, *Nat. Mater.* 2015, **14**, 1245.

13 Y. Yin, J. Han, Y. Zhang, X. Zhang, P. Xu, Q. Yuan, L. Samad, X. Wang, Y. Wang, and Z. Zhang, *J. Am. Chem. Soc.* 2016, **138**, 7965–7972.

14 X. Yu, Y. Feng, Y. Jeon, B. Guan, X. W. Lou and U.Paik, *Adv. Mater.* 2016, **28**, 9006–9011.

15 L. Yu, B. Y. Xia, X. Wang and X. W. Lou, *Adv. Mater.* 2016, **28**, 92–97.

16 J. Duan, S. Chen, B. A. Chambers, G. G. Andersson and S. Z. Qiao, *Adv. Mater.* 2015, **27**, 4234–4241.

17 J. Xie, S. Li, X. Zhang, J. Zhang, R. Wang, H. Zhang, B. Pan and Y. Xie, *Chem. Sci.* 2014, **5**, 4615–4620.

18 H. Zhou, F. Yu, Y. Huang, J. Sun, Z. Zhu, R. J. Nielsen, R. He, J. Bao, W. A. Goddard III, S. Chen and Z. Ren, *Nat. Commun.* 2016, **7**, 12765.

19 Y. Liu, X. Hua, C. Xiao, T. Zhou, P. Huang, Z. Guo, B. Pan and Y. Xie, *J. Am. Chem. Soc.* 2016, **138**, 5087–5092.

20 L. Liang, H. Cheng, F. Lei, J. Han, S. Gao, C. Wang, Y. Sun, S. Qamar, S. Wei and Y. Xie, *Angew. Chem. Int. Ed.* 2015, **54**, 12004–12008.

21 F.-X. Ma, H. B. Wu, B. Y. Xia, C.-Y. Xu and X. W. D. Lou, *Angew. Chem. Int. Ed.* 2015, **54**, 15395–15399.

22 C. Zhu, S. Fu, Q. Shi, D. Du, Y. Lin. *Angew. Chem. Int. Ed.* 2017, **56**, 13944-13960.

23 H. Zhang, G. Liu, L. Shi, J. Ye, *Adv. Energy Mater.* 2018, **8**, 1701343.

24 B. Qiao, A. Wang, X. Yang, L. F. Allard, Z. Jiang, Y. Cui, J. Liu, J. Li, and T. Zhang, *Nat. Chem.* 2011, **3**, 634.

25 G. Gao, Y. Jiao, E. R. Waclawik and A. Du, *J. Am. Chem. Soc.* 2016, **138**, 6292–6297.

26 X.-K. Gu, B. Qiao, C.-Q. Huang, W. -C. Ding, K. Sun, E. Zhan, T. Zhang, J. Liu and W. -X. Li, *ACS Catal.* 2014, **4**, 3886–3890.

27 M. Moses-DeBusk, M. Yoon, L. F. Allard, D. R. Mullins, Z. Wu, X. Yang, G. Veith, G. M. Stocks and C. K. Narula, *J. Am. Chem. Soc.* 2013, **135**, 12634–12645.

28 J. Deng, H. Li, J. Xiao, Y. Tu, D. Deng, H. Yang, H. Tian, J. Li, P. Ren and X. Bao, *Energy & Environ. Sci* 2015, **8**, 1594–1601.

29 J. Jones, H. Xiong, A. T. DeLaRiva, E. J. Peterson, H. Pham, S. R. Challa, G. Qi, S. Oh, M. H. Wiebenga, X. I. P. Hernández, Y. Wang and A. K. Datye, *Science* 2016, **353**, 150–154.

30 L. Lin, W. Zhou, R. Gao, S. Yao, X. Zhang, W. Xu, S. Zheng, Z. Jiang, Q. Yu and Y.-W.Li, *Nature* 2017, **544**, 80.

31 Y. Han, Y. –G. Wang, W. Chen, R. Xu, L. Zheng, J. Zhang, J. Luo, R. –A. Shen, Y. Zhu, W. –C. Cheong, C. Chen, Q. Peng, D. Wang and Y. Li, *J. Am. Chem. Soc.* 2017, **139**, 17269-17272.

32 J. Wang, Z. Huang, W. Liu, C. Chang, H. Tang, Z. Li, W. Chen, C. Jia, S. Wei and Y. Li, *J. Am. Chem. Soc.* 2017, **139**, 17281-17284.

33 Y. Chen, S. Ji, Y. Wang, J. Dong, W. Chen, Z. Li, R. Shen, L. Zhen, Z. Zhuang, D. Wang and Y. Li, *Angew. Chem. Int. Ed.* 2017, **56**, 6937-6941.

34 M. Zhang, Y. –G. Wang, W. Chen, J. Dong, L. Zheng, J. Luo, J. Wan, S. Tian, W. –C. Cheong, D. Wang and Y. Li, *J. Am. Chem. Soc.* 2017, **139**, 10976-10979.

35 W. Chen, J. Pei, C. –T. He, J. Wan, H. Ren, Y. Zhu, Y. Wang, J. Dong, S. Tian, W. –C. Cheong, S. Lu, L. Zheng, W. Yan, Z. Zhuang, C. Chen, Q. Peng, D. Wang and Y. Li, *Angew. Chem. Int. Ed.* 2017, **56**, 16086-16090.

36 C. J. Lei, Y. Wang, Y. Hou, P. Liu, J. Yang, T. Zhang, X. D. Zhuang, M. W. Chen, B. Yang, L. C. Lei, C. Yuan, X. L. Feng. Energy. Environ. Sci. DOI: 10.1039/C8EE01841C

37. Z. G. Geng, Y. Liu, X. D. Kong, P. Li, K. Li, Z. Y. Liu, J. J. Du, M. Shu, R. Si, J. Zeng. Adv. Mater. 2018, 30, 1803498.

38. Y. T. Qu, Z. J. Li, W. X. Chen, Y. Lin, T. W. Yuan, Z. K. Yang, C. M. Zhao, J. Wang, C. Zhao, X. Wang, F. Y. Zhou, Z. B. Zhuang, Y. Wu, Y. D. Li. Nat. Catal. 2018, 1, 781-786.

39 Y. Jiang, Y. Lu, X. Lv, D. Han, Q. Zhang, L. Niu and W. Chen, *ACS Catal.* 2013, **3**, 1263-1271.

40 Y. Zhang, X. Fan, J. Jian, D. Yu, Z. Zhang and L. Dai, *Energy. Environ. Sci.* 2017, **10**, 2312-2317.

41 J. Bao, X. Zhang, B. Fan, J. Zhang, M. Zhou, W. Yang, X. Hu, H. Wang, B. Pan and Y. Xie, *Angew. Chem. Int. Ed.* 2015, **127**, 7507–7512.

42 Y. E. Roginskaya, O. Morozova, E. Lubnin, Y. E. Ulitina, G. Lopukhova and S. Trasatti, *Langmuir* 1997, **13**, 4621–4627.

43 A. Mansour, J. Cook Jr and D. Sayers, *J. Phys. Chem.* 1984, **88**, 2330–2334.

44 T. Sham, S. Naftel and I. Coulthard, *J. Appl. Phys.* 1996, **79**, 7134–7138.

45 P. Wang, X. Zhang, J. Zhang, S. Wan, S. Guo, G. Lu, J. Yao and X. Huang, *Nat. Commun.* 2017, **8**, 14580.

46 S. Wang, X. Gao, X. Hang, X. Zhu, H. Han, W. Liao and W. Chen, *J. Am. Chem. Soc.* 2016, **138**, 16236–16239.

47 X. Xie, Y. -F. Jiang, C. -Z. Yuan, N. Jiang, S. -J. Zhao, L. Jia and A. -W. Xu, *J. Phys. Chem. C* 2017, **121**, 24979–24986.

48 S. Anantharaj, P. E. Karthik, B. Subramanian and S. Kundu, *ACS Catal.* 2016, **6**, 4660–4672.

49 A. B. Soliman, M. H. Hassan, T. N. Huan, A. A. Abugable, W. A. Elmehalmey, S. G. Karakalos, M. Tsotsalas, M. Heinle, M. Elbahri, M. Fontecave and M. Alkordi, *ACS Catal.* 2017, **7**, 7847–7854.

50 P. Wang, K. Jiang, G. Wang, J. Yao and X. Huang, *Angew. Chem.* 2016, 128, 13051–13055.

51 N. Cheng, S. Stambula, D. Wang, M. Banis, T. Liu, A. Riese, B. Xiao, R. Li, T, Sham, M. Liu, G. Botton and X. Sun, *Nat. Commun.* 2016, **7**, 13638.

52 H. Wei, K. Huang, D. Wang, R. Zhang, B. Ge, J. Ma, B. Wen, S. Zhang, Q. Li, M. Lei, C, Zhang, J. Irawan, L. Liu and H, Wu. *Nat. Commun.* 2017, **8**, 1490.

53 X. Yin, H. Wang, S. Tang, X. Lu, M. Shu, R. Si and T. Lu. *Angew. Chem. Int. Ed.* 2018, **57**, 9382-9386

54 Y. Shi and B. Zhang, *Chem. Soc. Rev.* 2016, **45**, 1529-1541.

55 Z. Chen, Y. Song, J. Cai, X. Zheng, D. Han, Y. Wu, Y. Zang, S. Niu, Y. Liu, J. Zhu, X. Liu and G, Wang. *Angew. Chem. Int. Ed.* 2018, **57**, 5076-5080.

56 L. Zhang, Y. Jia, G. Gao, X. Yan, N. Chen, J. Chen, M. Soo, B. Wood, D. Yang, A. Du and X. Yao. *Chem.* 2018, **4**, 285-297.

57 W. Chen, J. Pei, C. He, J. Wan, H. Ren, Y. Zhu, Y. Wang, J. Dong, S. Tian, W. Cheong, S. Lu, L. Zheng, X. Zheng, W. Yan, Z. Zhuang, C. Chen, Q. Peng, D. Wang and Y. Li. *Angew. Chem. Int. Ed.* 2017, **56**, 16086-16090.

58 Y. Jiao, Y. Zheng, K. Davey and S. Qiao, *Nat. Energy.* 2016, **1**, 16130.

View Article Online
DOI: 10.1039/C8EE02888E

59 Y. Jiao, Y, Zheng, M. Jaroniec and S. Qiao, *Chem. Soc. Rev.* 2015, **44**, 2060-2068.
60 M. D. Segall, P. J. D. L. M. J. Probert, C. J. Pickard, P. J. Hasnip, S. J. Clark and M. C. Payne, *J. Phys.: Condens. Matter* 2002, **14**, 2717-2744.
61 J. P. Perdew, K. Burke and M. Ernzerhof, *Phys. Rev. Lett.* 1996, **77**, 3865-3868
62 D. R. Hamann and M. Schl¨ uter, C. Chiang, *Phys. Rev. Lett.* 1979, **43**, 1494-1497.
63 D. Voiry, H. Yamaguchi, J. Li, R. Silva, D. C. B. Alves, T. Fujita, M. W. Chen, T. Asefa, V. Shenoy, G. Eda and M. Chhowalla, *Nat. Mater.* 2013, **12**, 850-855.